

From Seeing to Experiencing: Scaling Navigation Foundation Models with Reinforcement Learning

Honglin He*, Yukai Ma*, Wayne Wu, Bolei Zhou

University of California, Los Angeles

<https://metadriverse.github.io/s2e>

Abstract: Navigation foundation models trained on massive web-scale data enable agents to generalize across diverse environments and embodiments. However, these models, which are trained solely on offline data, often lack the capacity to reason about the consequences of their actions or adapt through counterfactual understanding. They thus face significant limitations in the real-world urban navigation where interactive and safe behaviors, such as avoiding obstacles and moving pedestrians, are critical. To tackle these challenges, we introduce the Seeing-to-Experiencing (S2E) learning framework to scale the capability of navigation foundation models with reinforcement learning. S2E combines the strengths of pre-training on offline videos and post-training through reinforcement learning. It maintains the model’s generalizability acquired from large-scale real-world videos while enhancing its interactivity through reinforcement learning in simulation environments. Specifically, we introduce two innovations: 1) an Anchor-Guided Distribution Matching strategy for offline pretraining, which stabilizes learning and models diverse motion patterns through anchor-based supervision; and 2) a Residual-Attention Module for reinforcement learning, which obtains reactive behaviors from simulation environments without erasing the model’s pretrained knowledge. Moreover, we establish a comprehensive end-to-end evaluation benchmark, NavBench-GS, built on photorealistic 3D Gaussian Splatting reconstructions of real-world scenes that incorporate physical interactions. It can systematically assess the generalizability and safety of navigation foundation models. Extensive experiments show that S2E mitigates the diminishing returns often seen when scaling with offline data alone. We perform a thorough analysis of the benefits of Reinforcement Learning (RL) compared to Supervised Fine-Tuning (SFT) in the context of post-training for robot learning. Our findings emphasize the crucial role of integrating interactive online experiences to effectively scale foundation models in Robotics.

Keywords: Urban Navigation, Foundation Models, Reinforcement Learning



Real-world deployments of S2E on wheeled and quadruped robots

Figure 1: Real-world deployments of S2E. S2E achieves zero-shot generalization across environments and embodiments. We demonstrate its effectiveness on wheeled and quadruped robots in diverse urban scenarios.

*Equal contribution.

1 Introduction

Foundation models have demonstrated transformative capabilities across various domains, including language understanding [1, 2], generation [3, 4], and visual recognition [5–7]. Through training on massive data, these models significantly enhance the generalizability and adaptability of downstream tasks. However, applying foundation models to robot navigation presents unique challenges [8] due to the complex nature of sequential decision-making in dynamic real-world environments. For example, in a hustling urban space, navigation foundation models must make real-time decisions to avoid collision with obstacles like trash bins and safely maneuver through ever-changing crowds.

Recent work on navigation foundation models has harnessed large-scale web videos and human demonstrations for pretraining [9–11]. These approaches primarily rely on passive visual learning [12, 13], where models are trained to imitate behaviors observed in massive video data. Such data captures diverse visual observations of the real world; yet, it lacks explicit information on physics and cause-effect relations, which are crucial for decision-making in the real world. As a result, navigation policies trained solely on offline data often exhibit limited *reactivity* to the surroundings and struggle to adapt to dynamic objects and motions in the environment.

While *offline* video data helps build proper perceptual prior for the model, it only captures statistical correlations, not grounded causality [14]. Visual imitation [15, 16] teaches an agent what actions look like, but *not* how to adapt, recover, or reason about counterfactual outcomes when the environment changes. Thus, navigation foundation models must move **from seeing to experiencing**: *actively* interact with the world, receive feedback, and refine behaviors through trial and error. As shown in Figure 2, similar to humans learning skateboarding, where experience with balance, falling, and correction is irreplaceable, agents must interact with the world to acquire true adaptability. Reinforcement Learning (RL) enables agents to close the gap between observations and actions and offers a scalable interactive learning paradigm to enrich model capabilities beyond the behavior cloning of static datasets. However, RL alone has shown limited success in building generalizable navigation models. Prior approaches [17–21] have trained agents in narrow synthetic environments through RL; however, due to the poor sampling efficiency and lack of inductive priors, the resulting models are struggling to achieve scalable and generalizable navigation capabilities in the real world.

To this end, we propose a new learning framework, **Seeing-to-Experiencing (S2E)**, to scale navigation foundation models with reinforcement learning in simulated environments while maintaining the generalizable visual representation acquired through pretraining on offline videos. This framework comprises two crucial technical components. First, we introduce an Anchor-Guided Distribution Matching (AGDM) strategy for pre-training on real-world video data. It is designed as an anchor-guided model architecture to learn complex multi-modal distributions in normalized motion trajectory space, enabling efficient representation of diverse behaviors across scenarios. This design significantly mitigates learning uncertainty and provides a more reliable backbone to ease subsequent online adaptation. Moreover, the anchor-based architecture naturally supports the cross-embodiment deployment of the foundation model. Second, we propose a Residual-Attention Module (RAM) for RL post-training in simulation environments. It is designed as a residual architecture by copying the pretrained attention block and learning a residual component that selectively captures knowledge acquired from online interactions. This design allows agents to obtain novel capabilities, such as obstacle avoidance and movement anticipation, through reinforcement learning while preserving the generalizable visuomotor representations learned from offline pretraining.

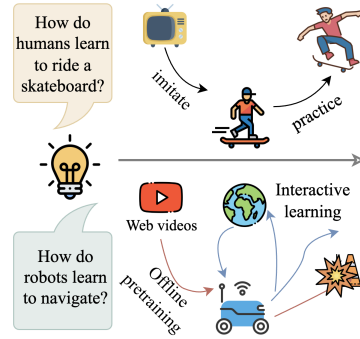


Figure 2: Motivation. Like humans, AI agents must also go through interactive practices and learn from feedback to obtain actionable skills.

We further introduce NavBench-GS, a comprehensive end-to-end evaluation benchmark built on realistic 3D Gaussian Splatting environments with accurate physics and interactive dynamics. Unlike prior evaluations that rely on offline 2D video-based testing [9–11], NavBench-GS enables the

reactive simulation to facilitate closed-loop policy assessment in photo-realistic 3D scenes. These scenes, combining realistic visual appearance and physical interaction with reproducibility, address a longstanding challenge in robotics: the difficulty of replicating real-world environments for end-to-end evaluation. It enables standardized, reproducible evaluation of navigation foundation models in terms of generalization and safety in unseen settings.

Extensive experiments show that reinforcement learning substantially enhances the policy performance and alleviates the diminishing returns associated with scaling solely on offline data. We analyze the effectiveness of Reinforcement Learning (RL) versus Supervised Fine-Tuning (SFT) in post-training for robot learning. Although both methods are widely discussed in relation to large language models (LLMs) [22], they remain underexplored in the field of scaling robot learning. Additionally, we demonstrate the generalizability of the proposed S2E framework through real-world evaluations in challenging scenarios.

2 Related Work

Goal conditioned navigation. Goal-conditioned navigation is the most common setting for robotic navigation. Prior works have developed diverse approaches to represent navigation goals, which can be categorized into three main paradigms: 1) image-goal navigation, where target images serve as visual references [23–25]; 2) position-goal navigation, which directly encodes destination coordinates [26–28]; and 3) object-goal navigation, where targets are specified through object categories [29–31]. Deep reinforcement learning [32] has demonstrated promising results in mapless navigation by eliminating dependency on maps. However, these methods often suffer from limited generalization, particularly in visual navigation [17–19], due to the constrained diversity of training scenarios. The synthetic nature and restricted variation in simulated training worlds inherently limit the policy’s ability to adapt to real-world complexity and unseen scenarios.

Navigation foundation models. Many recent works have proposed various vision-based navigation foundation models [9–11], leveraging advantages in cross-sensor capabilities and rich vision data for improved generalizability across different robot platforms and camera configurations. CityWalker [33] and NWM [34] further enhance the environmental comprehension of policy by incorporating future state prediction, enabling more informed navigation decisions. However, a key limitation of such approaches is the lack of environmental interactions in the training data, which, as we demonstrate in Section 4.2, results in poor obstacle and pedestrian avoidance performance. To address this, it is essential to develop policies that are generalizable and capable of high-quality local planning, rather than relying solely on path-following capabilities.

Hybrid learning with pretraining and finetuning. The paradigm of offline pretraining followed by RL fine-tuning has emerged as a powerful framework for training robust control policies, bridging the gap between data efficiency and real-world adaptability. Early successes in playing games, such as AlphaGo [35] and AlphaStar [36], demonstrated the potential of combining large-scale pretraining (*e.g.*, supervised learning from expert trajectories) with RL fine-tuning to achieve superhuman performance. This approach has since been extended to train foundation models, where pretrained LLMs [1, 37] and VLMs [38] are fine-tuned via Reinforcement Learning from Human Feedback (RLHF) to align with human values and preferences.

3 S2E Learning Framework

To address the challenge of training generalizable and interactive foundation navigation models, we propose **S2E**, a hybrid learning framework that combines pretraining on videos and reinforcement learning in simulated environments. Figure 3 illustrates the overall framework of the proposed S2E. It aims to learn a visual navigation policy π that enables a robot to navigate from the source waypoint coordinate p_s to the target waypoint coordinate p_d . This task focuses on local navigation [25, 33] between consecutive waypoints, which can be easily extended to long-distance tasks by chaining waypoints obtained from path planning [39]. At each timestep t , the observations are RGB frames $\mathbf{o}_{t-k+1:t}$ spanning the past k frames, and the target coordinates p_d . The output is a short-term relative waypoint as its action a at a frequency of 5Hz, then locomotion models can execute it

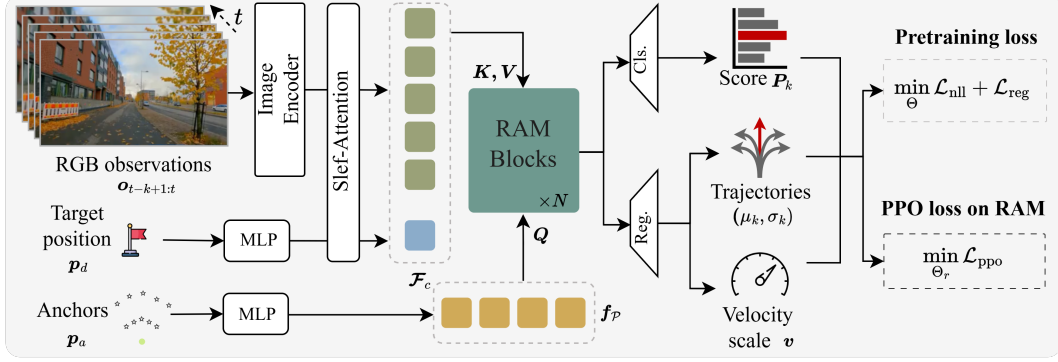


Figure 3: Illustration of S2E framework. The model receives continuous RGB frames and the target position as context information and utilizes pre-defined embodiment-agnostic anchors as queries for prediction. First, context embeddings are integrated via a self-attention module. The outputs are then used as keys (K) and values (V). Meanwhile, the anchor features f_P serve as queries (Q). Subsequently, RAM blocks compute weighted features from K and V based on the anchor queries Q , and produce refined anchor features. A classification and a regression head decode the anchor features to predict scores and normalized trajectories with a velocity scale. In the pretraining stage, the model is trained end-to-end with NLL and regression loss (Equation 2). In the finetuning stage, only the parameters within the RAM blocks are optimized with policy gradient.

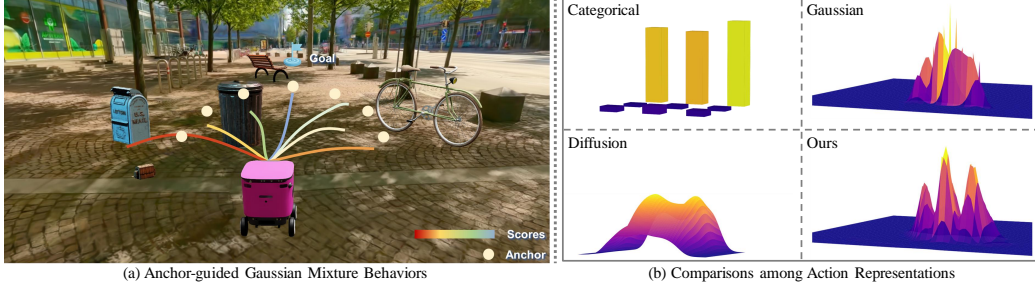


Figure 4: Illustration of anchor-guided distribution matching. (a) Illustration of anchor-guided Gaussian Mixture behaviors in a sidewalk scenario, where anchors guide diverse behavior generation. (b) Comparison of predicted action distributions between different representations.

to move the robot incrementally toward the goal. Our framework consists of two key technical components: 1) anchor-guided distribution matching for robust backbone pretraining (Section 3.1) for pretraining, and 2) Residual-Attention Module for capability injection with RL (Section 3.2).

3.1 Pretraining with Anchor-Guided Distribution Matching

A robust backbone for extracting meaningful visual features is essential for generalization across diverse scenarios. We pretrain our model on 35 hours of navigation videos collected from various robots and platforms [40–44], covering a wide range of environments. However, modeling *multi-modal data distributions* still presents significant challenges [11], as the model must generate diverse predictions under the same conditions. To address this, we introduce the anchor-guided distribution matching detailed in the following section.

Anchor-guided distribution matching. Robot navigation trajectories are inherently multimodal – given the same observation, multiple distinct actions may be valid. Effectively modeling this multimodality is crucial for generalizable policies. However, common representations like discrete actions [45] or unimodal Gaussians [9, 10, 33] lack expressiveness, limiting the model to capture the information from partial observation, the accumulation of prediction errors over time [46], etc. While diffusion models [11, 47], though expressive, are overly flexible and difficult to control in navigation, often yielding fragmented trajectories that compromise safety and stability.

To address this, we propose an anchor-guided Gaussian Mixture Model (GMM) [48, 49] to represent robot actions in urban navigation, as illustrated in Figure 4 (a). This formulation offers both multimodality and structure. Anchors, uniformly sampled in the robot’s forward direction, serve as interpretable high-level intentions. Each anchor corresponds to a Gaussian mode in the mixture, with



Figure 5: Overview of training environments and evaluation benchmark. (a) Real-world data pretraining has realistic appearances but lacks interactions. (b) Synthetic data from RL simulation supplements rich physical interactions. (c) Scene in NavBench-GS offers realistic visual appearances and physical interactions for end-to-end evaluation.

learned scores reflecting likelihoods. The policy learns to generate and choose trajectories based on these anchors, enabling diverse yet goal-aligned behaviors. This approach combines expressiveness with training stability and is also well-suited for fine-tuning with reinforcement learning.

We present the distributions of actions using various representations in Figure 4 (b), including categorical, unimodal Gaussians, diffusion policy, and our anchor-guided Gaussian Mixture Model (GMM). The categorical representation learns actions in discretized bins, which restricts its ability to capture nuanced or multimodal behavior. The unimodal Gaussian representation tends towards a single modal distribution, making it ineffective in capturing the multiple valid actions in trajectories. The diffusion policy learns a smooth and comprehensive distribution, but is too flexible, which complicates the guidance and control of behaviors. Our anchor-guided GMM provides a structured, multi-modal distribution where different anchors specialize in different high-level intentions (*e.g.*, go straight, turn, yield). Also, the model retains intra-mode uncertainty by allowing moderate variance within each anchor’s predicted distribution with a learned standard deviation.

The model architecture for distribution matching is illustrated in Figure 3. Specifically, we generate M representative intention points $\mathbf{p}_a \in \mathbb{R}^{M \times 2}$ by uniform sampling, which serves as an additional input beyond RGB frames and target position. The distribution of the action w_t at timestep t under observation $\mathbf{o}_{t-k+1:t}$ is a Gaussian Mixture Model (GMM) defined as:

$$\mathbf{q}(w_t | \mathbf{o}_{t-k+1:t}) = \sum_{m=1}^M q_m \cdot \mathcal{N}_m(w_x - \mu_x^m, \sigma_x^m; w_y - \mu_y^m, \sigma_y^m; \rho^m), \quad (1)$$

where the score distribution q_m denotes the probability of each intention point \mathbf{p}_a^m being selected as the guiding mode for action prediction, $\mathbf{w}_t = (w_x, w_y)$ denotes the position variables as input of the locomotion to generate action a . $\mu_{x/y}^m$, $\sigma_{x/y}^m$, and ρ^m denote the mean, standard deviation, and correlation predicted by the m -th trajectory head, respectively. To convert normalized displacements into real-world behavior, we predict a scale $v \in \mathbb{R}^+$ per mode, allowing the policy to model absolute trajectory magnitude while preserving directionality.

Training process. The model is trained end-to-end with two training losses. The first is the Negative Log-Likelihood (NLL) loss as shown in Equation 2 used to supervise both the classification and trajectory heads. Inspired by [49], we employ an assignment strategy that selects the mode whose predicted direction best aligns with the ground-truth trajectory for optimization. The second loss is an L2 regression loss used to optimize the velocity scale.

$$\mathcal{L}_{nll} = -\log \mathcal{N}_h(\hat{w}_x - \mu_x^h, \sigma_x^h; \hat{w}_y - \mu_y^h, \sigma_y^h; \rho^h) - \log(q_h), \quad (2)$$

$$\mathcal{L}_{reg} = \|\hat{v} - v\|_2^2, \quad (3)$$

where the selected mode h is the one whose anchor is closest to the ground truth and chosen for optimization. More details are provided in the [Appendix](#).

3.2 Reinforcement Learning with Residual Attention Module

A naive solution for the trained model to obtain interactivity is fine-tuning the full model parameters in simulation. However, this can specialize the learned representations to synthetic images and cause *distributional drift* from real-world data. This is especially critical for sensitive components

like visual encoders, which may degrade significantly when being trained solely on simulated data. To address this challenge, we introduce a Residual Attention Module in the following section.

Residual attention module. Before presenting our finetuning approach, we first analyze which architectural components are both 1) tightly coupled with agent-environment interaction and 2) relatively invariant to sim-to-real gaps—these constitute our target modules for adaptation. Visual encoders ϕ_V and self-attention layers ψ_E primarily process scene context features, making them particularly sensitive to domain shifts [11, 50, 51]. In contrast, cross-attention layers ψ_D explicitly model agent-environment interactions, and these relational patterns remain consistent across domains. Therefore, we identify cross-attention layers as the key components tightly coupled with interactions but relatively robust to the sim-to-real gap, making them suitable for finetuning in simulation environments.

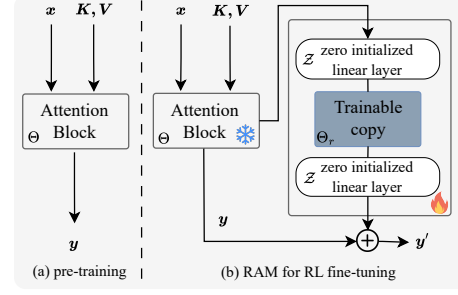


Figure 6: Residual attention module.

To fine-tune this interaction-related layer effectively, we introduce **Residual-Attention Module (RAM)**, which is initialized from the original pretrained weights while keeping the original modules frozen, as shown in Figure 6, inspired by previous works [52–55]. Instead of directly optimizing the pretrained weights, RAM maintains a parallel copy of the layers and performs fine-tuning on this copy. Formally, suppose the transformer decoder that we trained on real-world datasets as $\psi_D(Q; K, V; \Theta)$ with parameters Θ that transforms the input query x to y , i.e., $y = \psi_D(x; K, V; \Theta)$. To incorporate RAM into the pretrained module, we freeze the original parameters Θ of the target block and create a trainable copy with parameters Θ_t . This copied block is wrapped by two zero-initialized linear layers placed before and after the cloned module. Such a design ensures that, at initialization, the added adaptation branch has no effect on the original model output, while allowing smooth adaptation during finetuning as the zero-linear layers Z gradually learn to modulate the interaction-related features, i.e., $y' = y + Z(\psi_D(Z(y); K, V; \Theta_t))$.

Training process. The model is trained by PPO [56] with 256 parallel environments, each containing obstacles randomly distributed within a 30×30 region. Some samples of training environments are shown in Figure 5 (b). We define the reward function as $R = R_{vel} + R_{dis} + R_{arrive} + R_{collision}$, where R_{vel} measures the cosine similarity between the agent’s velocity direction and the target direction, encouraging aligned motion. R_{dis} penalizes the displacement of the agent at each timestep. R_{arrive} and $R_{collision}$ are terminal rewards, given when the agent reaches the goal or collides with any obstacle, respectively. The policy gradient is used to adjust the parameters Θ_r of RAM. We use the standard PPO clipped objective \mathcal{L}_{ppo} with entropy regularization \mathcal{H}_π for fine-tuning:

$$\mathcal{L}_{ppo} = \mathbb{E}_t[\min(r_t \hat{A}_t, \text{clip}(r_t, 1 - \epsilon, 1 + \epsilon) \hat{A}_t)], \quad (4)$$

$$\mathcal{H}_\pi \approx \sum_{m=1}^M q_m \cdot \left[\frac{1}{2} \log[(2\pi e)^2 \sigma_x^{m2} \sigma_y^{m2}] \right] - \sum_{m=1}^M q_m \log q_m, \quad (5)$$

where $r_t = \frac{\pi(a_t|s_t)}{\pi_{old}(a_t|s_t)}$ is the probability ratio, \hat{A}_t is the estimated advantage, and ϵ is the clipping threshold. And the term \mathcal{H}_π is a simplified lower-bound approximation of the entropy of the GMM policy. Additional details are provided in the [Appendix](#).

4 Experiments

To better understand the role of RL in scaling up foundation models for navigation, we focus on the following key questions: **Q1:** Can RL post-training further boost navigation performance based on offline pre-training? **Q2:** What are the advantages of the S2E framework over other approaches? We address these questions through a series of experiments. Section 4.1 validates the effectiveness of RL in further scaling navigation foundation models. Section 4.2 benchmarks state-of-the-art navigation foundation models in realistic 3DGS scenes. Section 4.3 presents real-world evaluation results and demonstrates the generalizability of our method. Please refer to the [Appendix](#) for more details.

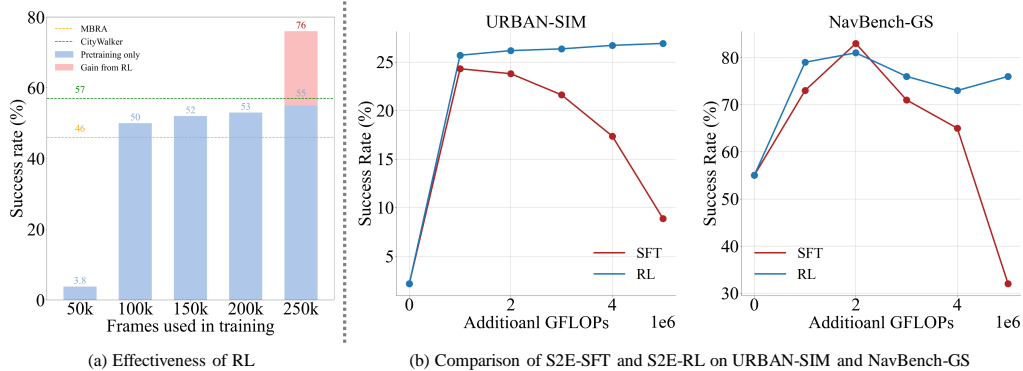


Figure 7: Effectiveness of reinforcement learning. (a) Success rates of policies trained with varying amounts of data, showing gain from RL fine-tuning over only supervised learning. Dotted lines indicate the performance of prior methods. (b) Performance comparison between SFT and RL policies under increasing training cost on URBAN-SIM. RL maintains robustness while SFT performance degrades as compute increases.

4.1 Scaling Up Model Performance via Reinforcement Learning

We first validate our motivation: while large-scale offline pre-training yields broad generalization, we investigate if RL can improve the performance after pretraining by enabling the model to learn from embodied interactions in simulation. Recent studies on scaling laws [57] suggest that model performance improves predictably with increasing data volume, model size, and compute budget. However, the diminishing returns are exhibited as the system approaches the scaling frontier [57]. As for the embodied navigation, this frontier arrives even earlier due to the relatively low-dimensional space of the action, the model quickly saturates its capacity to benefit from simply scaling in supervised learning. In large language models (LLMs), there have been numerous comparisons [22] between two different paradigms for post-training: Reinforcement Learning (RL) and Supervised Fine-Tuning (SFT). However, it remains unclear how post-training should be approached in the field of robot learning, especially as more scalable training methods are being developed in this domain [58].

To systematically study this phenomenon, we evaluate four model variants. 1) S2E-BC: A pure behavior cloning model trained solely on offline pretraining data. 2) S2E-PPO: A reinforcement learning agent trained from scratch with PPO. 3) S2E-SFT: An agent fine-tuned with data from URBAN-SIM [59] after pretraining. 4) S2E-Full: Our full approach combining pretraining followed by RL fine-tuning. Figure 7 shows that increasing the data scale for S2E-BC yields only marginal improvements beyond a certain point. Expanding the dataset from 100k to 200k samples results in a mere 3% increase in success rate. This indicates that more offline data is insufficient to enhance navigation capability further. In contrast, RL significantly enhances the model’s performance by leveraging embodied interactions in simulation, achieving a 21% improvement in success rate over the pretrained model, with no more offline data used. These results provide compelling evidence that RL can overcome the fundamental limitations of traditional scaling laws through.

Additionally, we compare the performance scaling of supervised fine-tuning (SFT) and reinforcement learning (RL) across two benchmarks in Figure 7 (b), including the in-distribution test in URBAN-SIM and the out-of-distribution test in NavBench-GS. The data used for SFT is collected via a pretrained policy interacting within the environment, and episodes involving collisions are removed to ensure training stability. As additional training cost increases, RL maintains or improves success rates, while SFT suffers from severe overfitting. These results show that RL is not only more sample-efficient, but also more robust under increased training cost.

4.2 NavBench-GS Benchmark

Although training durations and offline data sources vary between foundation models, our NavBench-GS benchmark remains fair and meaningful. We follow standard evaluation practice

Method	Video Data	Empty			Obstacle			Pedestrian			Obstacle + Pedestrian		
		SR \uparrow	RC \uparrow	CT \downarrow	SR \uparrow	RC \uparrow	CT \downarrow	SR \uparrow	RC \uparrow	CT \downarrow	SR \uparrow	RC \uparrow	CT \downarrow
ZeroPolicy	-	0.03	0.27	1.84	0.00	0.20	1.86	0.00	0.09	2.33	0.00	0.07	5.71
GNM [9]	70h	0.23	0.51	0.72	0.16	0.49	0.90	0.09	0.53	1.28	0.07	0.44	2.31
ViNT [10]	80h	0.28	0.51	0.60	0.13	0.46	1.21	0.07	0.48	1.22	0.08	0.39	1.99
NoMaD [11]	100h	0.15	0.46	<u>0.35</u>	0.11	0.44	0.89	0.09	0.48	0.68	0.08	0.42	1.83
ViNT* [10]	35h	0.80	0.81	0.49	0.61	0.78	1.18	0.28	0.71	2.17	0.03	0.33	4.84
NoMaD* [11]	35h	0.06	0.36	0.58	0.04	0.33	0.93	0.02	0.32	0.73	0.02	0.24	2.08
MBRA [60]	700h	0.61	0.75	<u>0.35</u>	0.46	0.63	0.50	0.32	0.66	0.79	0.24	0.61	1.61
CityWalker [33]	2000h	0.66	0.72	0.42	0.57	0.69	0.83	0.39	0.73	1.20	0.32	0.60	2.08
S2E-BC	35h	0.87	0.91	0.25	0.55	0.70	1.22	0.54	0.80	0.71	0.38	0.64	2.73
S2E-PPO	35h	0.05	0.12	1.73	0.02	0.10	2.37	0.04	0.12	1.94	0.01	0.08	4.94
S2E-SFT	35h	0.81	0.85	0.36	0.71	0.77	0.69	<u>0.55</u>	<u>0.86</u>	<u>0.61</u>	0.50	0.72	2.03
S2E-Full	35h	<u>0.83</u>	<u>0.87</u>	0.39	0.76	0.81	<u>0.56</u>	0.57	0.89	0.58	0.55	0.75	<u>1.81</u>

Table 1: NavBench-GS Benchmark. Comparison of navigation foundation models across four tasks.

in LLMs [2] and VLMs [38], where foundation models are frequently trained on different corpora due to data privacy concerns and distribution bias. In NavBench-GS, we keep all environments unseen and distributionally distant from the training data.

Benchmark. The core and foundational function for a robot in urban scenarios is to navigate from point A to point B. In this task, the main commands beyond reaching the goal include: 1) not collide with static objects and; 2) not crash with moving objects. To this end, we design a benchmark in photo-realistic and physically interactive scenarios from Vid2Sim [21], spanning 26 scenarios, each instantiated with 4 tasks, *i.e.*, 1) empty environments, 2) environments with random static obstacles, 3) environments with moving pedestrians, and 4) environments with obstacles and pedestrians. We use success rate (SR), route completion (RC) and collision times (CT) to measure the model performance. An episode is deemed successful if the robot reaches the destination with a remaining distance less than 1 meter, with fewer than 3 collisions with the obstacle or the pedestrian.

Baselines. To thoroughly evaluate our method’s advantages, we compare against several state-of-the-art navigation foundation models: 1) image-based approaches including GNM [9], ViNT [10], NoMaD [11], and 2) point-based approaches CityWalker [33], MBRA [60], ViNT* and NoMaD* (* denotes model re-trained with points as goal). And four variants of S2E as described before.

Results. As demonstrated in Table 1, S2E-Full consistently outperforms all baseline methods in both success rate and collision avoidance across all test scenarios, validating the effectiveness of our S2E framework. The performance gains are significant when comparing S2E-Full to S2E-BC, with success rate improvements of 21% in obstacle settings, 3% in pedestrian scenarios, and 17% in obstacle-pedestrian scenarios. These substantial improvements across increasingly complex environments demonstrate RL’s critical role in enhancing a policy’s interactive capabilities. Compared with point-based approaches, our results clearly show that scaling performance with RL is significantly more effective than simply scaling up the amount of training data.

4.3 Real-World Evaluations

For real-world evaluation, we use 5 real-world scenarios with a total of 8 routes, each repeated 3 times to test the model performance. We consider two types of environments: Empty, where only structural boundaries such as walls are present except for ground; Obstacle, where static objects are randomly placed between the agent’s starting point and the destination. We validate our approach through a comprehensive real-world evaluation using two distinct robotic platforms: 1) the Unitree GO2 quadrupedal robot, and 2) the COCO wheeled robot. Figure 8 provides a qualitative comparison between S2E-Full and baseline methods, clearly demonstrating S2E-Full’s superior collision avoidance capability in complex scenarios where other methods fail. Quantitative results in Table 2 further confirm these observations, with S2E-Full achieving the highest performance in both success rate and collision avoidance metrics. These results clearly illustrate that the interactive capabilities learned through RL training in simulation transfer effectively to the real world in a zero-shot manner.

Wheeled robot			
Method	SR \uparrow	RC \uparrow	CT \downarrow
NoMaD [11]	0.13	0.51	0.93
CityWalker [33]	0.35	0.48	0.83
S2E-BC	0.32	0.70	0.78
S2E-Full	0.42	0.65	0.70

Quadruped robot			
Method	SR \uparrow	RC \uparrow	CT \downarrow
NoMaD [11]	0.06	0.49	0.96
CityWalker [33]	0.30	0.58	<u>0.84</u>
S2E-BC	0.34	0.63	0.91
S2E-Full	0.50	0.67	0.75

Table 2: Real-world results.

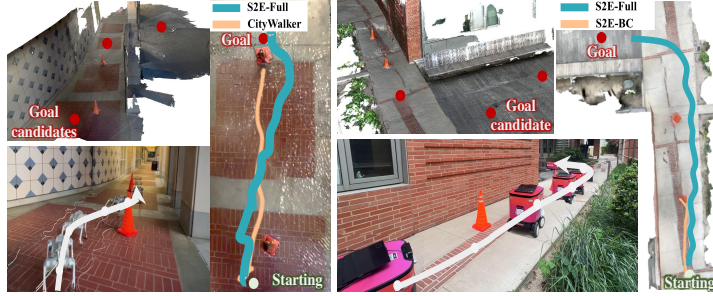


Figure 8: Visualization of real-world results.

5 Ablation Studies

In this section, we conduct ablation studies to evaluate the effectiveness of key components of our method, particularly the anchor-guided distribution matching and RAM for scaling with RL. More experiments such as generality across different embodiments can be found in the [Appendix](#).

Effectiveness of anchor guidance. As shown in Table 1, ViNT* [10] is trained with single-mode matching, while S2E-BC adopts anchor-guided distribution matching to model multi-modal distribution. Under the same setting, S2E-BC significantly outperforms ViNT* in both success rate (+33%) and collision rate (-2.11) in scenarios with obstacle and pedestrian, demonstrating that anchor-guided distribution matching improves the model ability to capture complex distributions.

Effectiveness of residual attention module. To evaluate the proposed learning under the limited-module setting, *i.e.*, RAM, we conduct ablation studies on different training strategies, where ‘‘S2E-FullIFT’’ indicates full-parameter fine-tuning from pretrained initialization. As shown in Table 3, our approach achieves the highest success rate and lowest collision times in NavBench-GS-Obstacle, demonstrating the effectiveness of our finetuning strategy under limited-module adaptation.

Methods	SR \uparrow	CT \downarrow
S2E-SFT	0.71	0.77
S2E-PPO	0.02	2.37
S2E-FullIFT	0.74	0.83
Ours	0.76	0.56

Table 3: Effectiveness of RAM.

6 Conclusion

We propose a novel Seeing-to-Experiencing (S2E) framework for learning navigation foundation models. It integrates an Anchor-Guided Distribution Matching strategy to adapt to diverse real-world conditions and a Residual-Attention Module (RAM) for incremental improvement in interactive learning. Extensive experiments demonstrate that the models trained from our framework achieve zero-shot transfer to unseen scenarios and can be seamlessly deployed across different robots.

7 Limitations and Future Work

Since current systems lack 3D perception, even our S2E-full model sometimes fails to avoid collisions, which remains a persistent challenge for vision-only navigation approaches. One potential solution is integrating depth estimation or occupancy (OCC) prediction tasks to infer 3D structural cues. Furthermore, the system encounters problems caused by the mechanical structures of the robot, such as the sim-to-real gap due to discrepancies between simulated and physical robotic platforms, and the performance degradation induced by locomotion control inaccuracies. Implementing higher-fidelity simulation modeling coupled with extensive data augmentation strategies may effectively mitigate these issues by reducing noise-related interference. In the future, we also plan to extend the proposed framework to other robotic applications such as mobile manipulation.

References

- [1] H. Touvron, T. Lavril, G. Izacard, X. Martinet, M.-A. Lachaux, T. Lacroix, B. Rozière, N. Goyal, E. Hambro, F. Azhar, et al. Llama: Open and efficient foundation language models. *arXiv preprint arXiv:2302.13971*, 2023. 2, 3
- [2] J. Bai, S. Bai, Y. Chu, Z. Cui, K. Dang, X. Deng, Y. Fan, W. Ge, Y. Han, F. Huang, et al. Qwen technical report. *arXiv preprint arXiv:2309.16609*, 2023. 2, 8
- [3] R. Rombach, A. Blattmann, D. Lorenz, P. Esser, and B. Ommer. High-resolution image synthesis with latent diffusion models, 2021. 2
- [4] B. Lin, Y. Ge, X. Cheng, Z. Li, B. Zhu, S. Wang, X. He, Y. Ye, S. Yuan, L. Chen, et al. Open-sora plan: Open-source large video generation model. *arXiv preprint arXiv:2412.00131*, 2024. 2
- [5] Z. Wang, Y. Li, X. Chen, S.-N. Lim, A. Torralba, H. Zhao, and S. Wang. Detecting everything in the open world: Towards universal object detection. In *Proceedings of the IEEE/CVF Conference on Computer Vision and Pattern Recognition*, pages 11433–11443, 2023. 2
- [6] A. Kirillov, E. Mintun, N. Ravi, H. Mao, C. Rolland, L. Gustafson, T. Xiao, S. Whitehead, A. C. Berg, W.-Y. Lo, et al. Segment anything. In *Proceedings of the IEEE/CVF international conference on computer vision*, pages 4015–4026, 2023.
- [7] L. Yang, B. Kang, Z. Huang, X. Xu, J. Feng, and H. Zhao. Depth anything: Unleashing the power of large-scale unlabeled data. In *Proceedings of the IEEE/CVF Conference on Computer Vision and Pattern Recognition*, pages 10371–10381, 2024. 2
- [8] R. Firoozi, J. Tucker, S. Tian, A. Majumdar, J. Sun, W. Liu, Y. Zhu, S. Song, A. Kapoor, K. Hausman, et al. Foundation models in robotics: Applications, challenges, and the future. *The International Journal of Robotics Research*, page 02783649241281508, 2023. 2
- [9] D. Shah, A. Sridhar, A. Bhorkar, N. Hirose, and S. Levine. Gnm: A general navigation model to drive any robot. In *2023 IEEE International Conference on Robotics and Automation (ICRA)*, pages 7226–7233. IEEE, 2023. 2, 3, 4, 8
- [10] D. Shah, A. Sridhar, N. Dashora, K. Stachowicz, K. Black, N. Hirose, and S. Levine. Vint: A foundation model for visual navigation. *arXiv preprint arXiv:2306.14846*, 2023. 4, 8, 9, 16
- [11] A. Sridhar, D. Shah, C. Glossop, and S. Levine. Nomad: Goal masked diffusion policies for navigation and exploration. In *2024 IEEE International Conference on Robotics and Automation (ICRA)*, pages 63–70. IEEE, 2024. 2, 3, 4, 6, 8, 9, 19, 23
- [12] M. J. Kim, K. Pertsch, S. Karamcheti, T. Xiao, A. Balakrishna, S. Nair, R. Rafailov, E. Foster, G. Lam, P. Sanketi, et al. Openvla: An open-source vision-language-action model. *arXiv preprint arXiv:2406.09246*, 2024. 2
- [13] A. Brohan, N. Brown, J. Carbajal, Y. Chebotar, J. Dabis, C. Finn, K. Gopalakrishnan, K. Hausman, A. Herzog, J. Hsu, et al. Rt-1: Robotics transformer for real-world control at scale. *arXiv preprint arXiv:2212.06817*, 2022. 2
- [14] D. Silver and R. S. Sutton. Welcome to the era of experience. *Google AI*, 2025. 2
- [15] Y. Dai, R. R. Sanchez, R. Jeronimus, S. Sagheb, C. M. Nunez, H. Nemlekar, and D. P. Losey. Civil: Causal and intuitive visual imitation learning. *arXiv preprint arXiv:2504.17959*, 2025. 2
- [16] H. Ren, Y. Zeng, Z. Bi, Z. Wan, J. Huang, and H. Cheng. Prior does matter: Visual navigation via denoising diffusion bridge models. *arXiv preprint arXiv:2504.10041*, 2025. 2

- [17] W. B. Shen, D. Xu, Y. Zhu, L. J. Guibas, L. Fei-Fei, and S. Savarese. Situational fusion of visual representation for visual navigation. In *Proceedings of the IEEE/CVF international conference on computer vision*, pages 2881–2890, 2019. 2, 3
- [18] P. Putta, G. Aggarwal, R. Mottaghi, D. Batra, N. Yokoyama, J. Truong, and A. Majumdar. Embodiment randomization for cross embodiment navigation. In *2024 IEEE/RSJ International Conference on Intelligent Robots and Systems (IROS)*, pages 5527–5534. IEEE, 2024.
- [19] J. Truong, D. Yarats, T. Li, F. Meier, S. Chernova, D. Batra, and A. Rai. Learning navigation skills for legged robots with learned robot embeddings. In *2021 IEEE/RSJ International Conference on Intelligent Robots and Systems (IROS)*, pages 484–491. IEEE, 2021. 3
- [20] K.-Y. Lin and S. X. Yu. Let humanoids hike! integrative skill development on complex trails. In *Proceedings of the Computer Vision and Pattern Recognition Conference*, pages 22498–22507, 2025.
- [21] Z. Xie, Z. Liu, Z. Peng, W. Wu, and B. Zhou. Vid2sim: Realistic and interactive simulation from video for urban navigation. *CVPR*, 2025. 2, 8
- [22] K. Kumar, T. Ashraf, O. Thawakar, R. M. Anwer, H. Cholakkal, M. Shah, M.-H. Yang, P. H. S. Torr, F. S. Khan, and S. Khan. Llm post-training: A deep dive into reasoning large language models, 2025. URL <https://arxiv.org/abs/2502.21321>. 3, 7
- [23] L. Mezghan, S. Sukhbaatar, T. Lavril, O. Maksymets, D. Batra, P. Bojanowski, and K. Alahari. Memory-augmented reinforcement learning for image-goal navigation. In *2022 IEEE/RSJ International Conference on Intelligent Robots and Systems (IROS)*, pages 3316–3323. IEEE, 2022. 3
- [24] S. K. Ramakrishnan, D. S. Chaplot, Z. Al-Halah, J. Malik, and K. Grauman. Poni: Potential functions for objectgoal navigation with interaction-free learning. In *Proceedings of the IEEE/CVF Conference on Computer Vision and Pattern Recognition*, pages 18890–18900, 2022.
- [25] Y. Zhu, R. Mottaghi, E. Kolve, J. J. Lim, A. Gupta, L. Fei-Fei, and A. Farhadi. Target-driven visual navigation in indoor scenes using deep reinforcement learning. In *2017 IEEE international conference on robotics and automation (ICRA)*, pages 3357–3364. IEEE, 2017. 3
- [26] D. S. Chaplot, D. Gandhi, S. Gupta, A. Gupta, and R. Salakhutdinov. Learning to explore using active neural slam. *arXiv preprint arXiv:2004.05155*, 2020. 3
- [27] P. Chattopadhyay, J. Hoffman, R. Mottaghi, and A. Kembhavi. Robustnav: Towards benchmarking robustness in embodied navigation. In *Proceedings of the IEEE/CVF International Conference on Computer Vision*, pages 15691–15700, 2021.
- [28] D. Gordon, A. Kadian, D. Parikh, J. Hoffman, and D. Batra. Splitnet: Sim2sim and task2task transfer for embodied visual navigation. In *Proceedings of the IEEE/CVF International Conference on Computer Vision*, pages 1022–1031, 2019. 3
- [29] Z. Al-Halah, S. K. Ramakrishnan, and K. Grauman. Zero experience required: Plug & play modular transfer learning for semantic visual navigation. In *Proceedings of the IEEE/CVF Conference on Computer Vision and Pattern Recognition*, pages 17031–17041, 2022. 3
- [30] M. Chang, A. Gupta, and S. Gupta. Semantic visual navigation by watching youtube videos. *Advances in Neural Information Processing Systems*, 33:4283–4294, 2020.
- [31] D. S. Chaplot, D. P. Gandhi, A. Gupta, and R. R. Salakhutdinov. Object goal navigation using goal-oriented semantic exploration. *Advances in Neural Information Processing Systems*, 33: 4247–4258, 2020. 3

- [32] P. Mirowski, R. Pascanu, F. Viola, H. Soyer, A. J. Ballard, A. Banino, M. Denil, R. Goroshin, L. Sifre, K. Kavukcuoglu, et al. Learning to navigate in complex environments. *arXiv preprint arXiv:1611.03673*, 2016. 3
- [33] X. Liu, J. Li, Y. Jiang, N. Sujay, Z. Yang, J. Zhang, J. Abanes, J. Zhang, and C. Feng. Citywalker: Learning embodied urban navigation from web-scale videos. *arXiv preprint arXiv:2411.17820*, 2024. 3, 4, 8, 9, 19
- [34] A. Bar, G. Zhou, D. Tran, T. Darrell, and Y. LeCun. Navigation world models. *arXiv preprint arXiv:2412.03572*, 2024. 3
- [35] D. Silver, A. Huang, C. J. Maddison, A. Guez, L. Sifre, G. Van Den Driessche, J. Schrittwieser, I. Antonoglou, V. Panneershelvam, M. Lanctot, et al. Mastering the game of go with deep neural networks and tree search. *nature*, 529(7587):484–489, 2016. 3
- [36] K. Arulkumaran, A. Cully, and J. Togelius. Alphastar: An evolutionary computation perspective. In *Proceedings of the genetic and evolutionary computation conference companion*, pages 314–315, 2019. 3
- [37] A. Halterman and K. A. Keith. Codebook llms: Evaluating llms as measurement tools for political science concepts, 2025. URL <https://arxiv.org/abs/2407.10747>. 3
- [38] Z. Chen, J. Wu, W. Wang, W. Su, G. Chen, S. Xing, M. Zhong, Q. Zhang, X. Zhu, L. Lu, et al. Internvl: Scaling up vision foundation models and aligning for generic visual-linguistic tasks. In *Proceedings of the IEEE/CVF conference on computer vision and pattern recognition*, pages 24185–24198, 2024. 3, 8
- [39] S. Thrun. Probabilistic robotics. *Communications of the ACM*, 45(3):52–57, 2002. 3
- [40] D. Shah, B. Eysenbach, G. Kahn, N. Rhinehart, and S. Levine. Rapid exploration for open-world navigation with latent goal models. *arXiv preprint arXiv:2104.05859*, 2021. 4, 17, 18, 19, 20
- [41] H. Karnan, A. Nair, X. Xiao, G. Warnell, S. Pirk, A. Toshev, J. Hart, J. Biswas, and P. Stone. Socially compliant navigation dataset (scand): A large-scale dataset of demonstrations for social navigation. *IEEE Robotics and Automation Letters*, 2022. 19, 20
- [42] H. Karnan, A. Nair, X. Xiao, G. Warnell, S. Pirk, A. Toshev, J. Hart, J. Biswas, and P. Stone. Socially Compliant Navigation Dataset (SCAND), 2022. URL <https://doi.org/10.18738/T8/OPRYRH>.
- [43] W. Liu, H. Zhao, C. Li, J. Biswas, B. Okal, P. Goyal, Y. Chang, and S. Pouya. X-mobility: End-to-end generalizable navigation via world modeling. *arXiv preprint arXiv:2410.17491*, 2024. 19, 20
- [44] W. Liu, H. Zhao, C. Li, J. Biswas, S. Pouya, and Y. Chang. Compass: Cross-embodiment mobility policy via residual rl and skill synthesis. *arXiv preprint arXiv:2502.16372*, 2025. 4, 19, 20
- [45] N. M. Shafiullah, Z. Cui, A. A. Altanzaya, and L. Pinto. Behavior transformers: Cloning k modes with one stone. *Advances in neural information processing systems*, 35:22955–22968, 2022. 4
- [46] F. Codevilla, E. Santana, A. M. López, and A. Gaidon. Exploring the limitations of behavior cloning for autonomous driving. In *Proceedings of the IEEE/CVF international conference on computer vision*, pages 9329–9338, 2019. 4
- [47] C. Chi, Z. Xu, S. Feng, E. Cousineau, Y. Du, B. Burchfiel, R. Tedrake, and S. Song. Diffusion policy: Visuomotor policy learning via action diffusion. *The International Journal of Robotics Research*, page 02783649241273668, 2023. 4

- [48] J. Gu, C. Sun, and H. Zhao. Densetnt: End-to-end trajectory prediction from dense goal sets. In *Proceedings of the IEEE/CVF International Conference on Computer Vision*, pages 15303–15312, 2021. 4
- [49] S. Shi, L. Jiang, D. Dai, and B. Schiele. Motion transformer with global intention localization and local movement refinement. *Advances in Neural Information Processing Systems*, 35: 6531–6543, 2022. 4, 5
- [50] J. Tobin, R. Fong, A. Ray, J. Schneider, W. Zaremba, and P. Abbeel. Domain randomization for transferring deep neural networks from simulation to the real world. In *2017 IEEE/RSJ international conference on intelligent robots and systems (IROS)*, pages 23–30. IEEE, 2017. 6
- [51] W. Zhao, J. P. Queralta, and T. Westerlund. Sim-to-real transfer in deep reinforcement learning for robotics: a survey. In *2020 IEEE symposium series on computational intelligence (SSCI)*, pages 737–744. IEEE, 2020. 6
- [52] L. Zhang, A. Rao, and M. Agrawala. Adding conditional control to text-to-image diffusion models. In *Proceedings of the IEEE/CVF international conference on computer vision*, pages 3836–3847, 2023. 6
- [53] C. Wu, Y. Gan, Y. Ge, Z. Lu, J. Wang, Y. Feng, Y. Shan, and P. Luo. Llama pro: Progressive llama with block expansion. *arXiv preprint arXiv:2401.02415*, 2024.
- [54] J.-B. Alayrac, J. Donahue, P. Luc, A. Miech, I. Barr, Y. Hasson, K. Lenc, A. Mensch, K. Millican, M. Reynolds, et al. Flamingo: a visual language model for few-shot learning. *Advances in neural information processing systems*, 35:23716–23736, 2022.
- [55] Y. Li, H. Liu, Q. Wu, F. Mu, J. Yang, J. Gao, C. Li, and Y. J. Lee. Gligen: Open-set grounded text-to-image generation. In *Proceedings of the IEEE/CVF conference on computer vision and pattern recognition*, pages 22511–22521, 2023. 6
- [56] J. Schulman, F. Wolski, P. Dhariwal, A. Radford, and O. Klimov. Proximal policy optimization algorithms. *arXiv preprint arXiv:1707.06347*, 2017. 6
- [57] J. Kaplan, S. McCandlish, T. Henighan, T. B. Brown, B. Chess, R. Child, S. Gray, A. Radford, J. Wu, and D. Amodei. Scaling laws for neural language models. *arXiv preprint arXiv:2001.08361*, 2020. 7
- [58] K. Black, N. Brown, D. Driess, A. Esmail, M. Equi, C. Finn, N. Fusai, L. Groom, K. Hausman, B. Ichter, et al. $\pi 0$: A vision-language-action flow model for general robot control. *arXiv preprint ARXIV.2410.24164*. 7
- [59] W. Wu, H. He, C. Zhang, J. He, S. Z. Zhao, R. Gong, Q. Li, and B. Zhou. Towards autonomous micromobility through scalable urban simulation. In *Proceedings of the IEEE/CVF Conference on Computer Vision and Pattern Recognition*, 2025. 7, 19, 20, 22
- [60] N. Hirose, L. Ignatova, K. Stachowicz, C. Glossop, S. Levine, and D. Shah. Learning to drive anywhere with model-based reannotation. *arXiv preprint arXiv:2505.05592*, 2025. 8
- [61] A. Radford, J. W. Kim, C. Hallacy, A. Ramesh, G. Goh, S. Agarwal, G. Sastry, A. Askell, P. Mishkin, J. Clark, et al. Learning transferable visual models from natural language supervision. In *International conference on machine learning*, pages 8748–8763. PmLR, 2021. 17
- [62] M. Oquab, T. Darcet, T. Moutakanni, H. Vo, M. Szafraniec, V. Khalidov, P. Fernandez, D. Haziza, F. Massa, A. El-Nouby, et al. Dinov2: Learning robust visual features without supervision. *arXiv preprint arXiv:2304.07193*, 2023. 17

- [63] G. Heinrich, M. Ranzinger, Y. Hongxu, Y. Lu, J. Kautz, A. Tao, B. Catanzaro, and P. Molchanov. Radiov2. 5: Improved baselines for agglomerative vision foundation models. In *Proc. CVPR*, volume 2, page 6, 2025. 17
- [64] M. Tan and Q. Le. Efficientnet: Rethinking model scaling for convolutional neural networks. In *International conference on machine learning*, pages 6105–6114. PMLR, 2019. 17, 18, 21
- [65] S. Ettinger, S. Cheng, B. Caine, C. Liu, H. Zhao, S. Pradhan, Y. Chai, B. Sapp, C. R. Qi, Y. Zhou, et al. Large scale interactive motion forecasting for autonomous driving: The waymo open motion dataset. In *Proceedings of the IEEE/CVF International Conference on Computer Vision*, pages 9710–9719, 2021. 17
- [66] J. Deng, W. Dong, R. Socher, L.-J. Li, K. Li, and L. Fei-Fei. Imagenet: A large-scale hierarchical image database. In *2009 IEEE conference on computer vision and pattern recognition*, pages 248–255. Ieee, 2009. 21
- [67] A. Vaswani, N. Shazeer, N. Parmar, J. Uszkoreit, L. Jones, A. N. Gomez, Ł. Kaiser, and I. Polosukhin. Attention is all you need. *Advances in neural information processing systems*, 30, 2017. 21
- [68] D. P. Kingma and J. Ba. Adam: A method for stochastic optimization. *arXiv preprint arXiv:1412.6980*, 2014. 21, 22
- [69] I. Loshchilov and F. Hutter. Decoupled weight decay regularization. *arXiv preprint arXiv:1711.05101*, 2017. 21, 22
- [70] M. F. Huber, T. Bailey, H. Durrant-Whyte, and U. D. Hanebeck. On entropy approximation for gaussian mixture random vectors. In *2008 IEEE International Conference on Multisensor Fusion and Integration for Intelligent Systems*, pages 181–188. IEEE, 2008. 22
- [71] Y. Wang, L. Wang, Y. Jiang, W. Zou, T. Liu, X. Song, W. Wang, L. Xiao, J. Wu, J. Duan, et al. Diffusion actor-critic with entropy regulator. *Advances in Neural Information Processing Systems*, 37:54183–54204, 2024. 22
- [72] J. Xu, V. Makoviychuk, Y. Narang, F. Ramos, W. Matusik, A. Garg, and M. Macklin. Accelerated policy learning with parallel differentiable simulation. *arXiv preprint arXiv:2204.07137*, 2022. 22, 23
- [73] V. S. Dorbala, J. F. Mullen, and D. Manocha. Can an embodied agent find your “cat-shaped mug”? IIm-based zero-shot object navigation. *IEEE Robotics and Automation Letters*, 9(5): 4083–4090, 2023. 22, 23
- [74] P. Polack, F. Altché, B. d’Andréa Novel, and A. de La Fortelle. The kinematic bicycle model: A consistent model for planning feasible trajectories for autonomous vehicles? In *2017 IEEE intelligent vehicles symposium (IV)*, pages 812–818. IEEE, 2017. 23

Appendix

A Demonstration Video

We highly recommend watching our supplementary video for detailed demonstrations. It presents a variety of experiments in both the simulator and the real world that thoroughly evaluate our S2E model across various settings and embodiments. *All real-world experiments conducted on different robots and scenes used the same S2E model.* The video consists of three sections:

- 1) S2E Capabilities Demonstration: highlights the ability of S2E in zero-shot deployment, including obstacle avoidance, interaction with pedestrians and long-horizon navigation.
- 2) Comparison with SOTA Methods: provides evaluations against representative baselines in real-world, demonstrating the performance of our method.
- 3) Data and Benchmark: introduces our training dataset for model pretraining, the interactive simulator used for policy finetuning, overview and results of the NavBench-GS benchmark.

B Real-World Experimental Results

In this section, we present experimental results in real-world scenarios, showcasing the zero-shot deployment performance of S2E. We first describe the setup and analysis of static obstacle evaluation in B.1, followed by experimental results involving dynamic human interactions with robots in B.2.

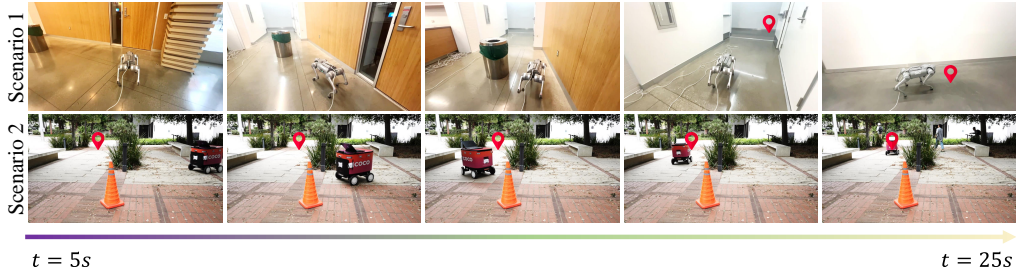


Figure 9: Evaluation on scenarios with static obstacles.

B.1 Scenarios with Static Obstacles

We placed objects along the robot’s path, such as a rubbish bin on the first row and a cone on the second row of Figure 9, to evaluate obstacle avoidance. Figure 9 demonstrates the performance of our S2E model in static obstacle scenarios: Scenario 1 illustrates GO2’s navigation in an indoor environment, while Scenario 2 shows COCO’s performance in an outdoor park setting with benches. The results confirm that our method reliably avoids obstacles.

B.2 Scenarios with Moving Pedestrians

We designed these experiments to evaluate robotic navigation capabilities in dynamic environments. In addition to static obstacles (*e.g.*, the cone shown in Figure 10), we introduced a dynamic scenario where a pedestrian walks toward the GO2 robot, forcing it to replan its path. As demonstrated in Figure 10, when the pedestrian obstructs the robot’s intended path, the robot dynamically adjusts its trajectory while still reaching the target destination.

C Additional Experimental Results

In this section, we present additional experiments to further analyze the framework design and effectiveness of S2E. We begin by validating the effectiveness of reinforcement learning in improving



Figure 10: Evaluation on scenarios with moving pedestrians.

other state-of-the-art methods [10] in C.1. We then measure the generalizability of the model across diverse embodiments in C.2, conduct ablations on the number of anchor points used for action prediction in C.3, and evaluate the impact of different visual backbones C.4. Furthermore, we provide qualitative results on the NavBench-GS benchmark in C.5.

C.1 Effectiveness of Reinforcement Learning

To validate the effectiveness of RL in improving performance, we conduct more studies between the pretrained model and its finetuned weights in the simulator. Specifically, we further conducted experiments on RL-based finetuning on top of ViNT* [10] introduced in manuscript, where only the policy head is updated while the backbone remains fixed. The setting of simulation environments, reward design, curriculum, etc. are consistent with the one used in S2E. As shown in results on Table 4, the finetuned policy outperforms the pretrained ViNT* across all evaluation metrics. Notably, it achieves significantly higher success rates and route completion, while also reducing collision cost. These results highlight the benefit of leveraging RL to continuously scale navigation foundation models that are trained solely on offline data.

Method	SR \uparrow	RC \uparrow	CT \downarrow
ViNT*	0.32	0.33	1.91
ViNT*+RL	0.49	0.61	1.02

Table 4: Performance comparison between pretrained and RL-finetuned on ViNT* [10]. Finetuning the policy using RL significantly improves navigation performance across all metrics, which demonstrates the effectiveness of reinforcement learning in scaling navigation performance.

C.2 Cross-Embodiment Generality

Robot Type	URBAN-SIM-Empty			NavBench-GS-Empty		
	SR \uparrow	RC \uparrow	SPL \uparrow	SR \uparrow	RC \uparrow	SPL \uparrow
Wheeled Robot	0.99 ± 0.06	0.99 ± 0.09	0.81 ± 0.26	0.92 ± 0.03	0.96 ± 0.02	0.90 ± 0.03
Quadruped Robot	0.93 ± 0.18	0.96 ± 0.10	0.91 ± 0.17	0.89 ± 0.08	0.89 ± 0.13	0.87 ± 0.08
Humanoid Robot	0.40 ± 0.16	0.75 ± 0.19	0.37 ± 0.19	0.21 ± 0.04	0.92 ± 0.09	0.18 ± 0.03

Table 5: Cross-embodiment generality. As a general navigation model, S2E can be directly deployed on various robotic platforms without any modifications.

Generalization across different embodiments is important for deploying or transferring policies in real-world applications. It would significantly reduce the retraining cost and improve the scalability of the model. To valid this capability, we evaluate the policy across three types of embodiments, *i.e.*, wheeled, quadruped and humanoid robots. We test two scenarios: simulation scenes generated

by URBAN-SIM and gaussian splatting scenes from NavBench-GS. As shown in Table 5, our approach maintains its performance across these different embodiments, showcasing the embodiment-agnostic property of the model. The wheeled and quadruped robots achieve high success rates, route completion, and SPL scores in all scenarios, demonstrating effective generalization across action controllers. While the humanoid robot shows lower success rate, its performance remains reasonable considering the increased joints. **Notably, all evaluations on both simulated and real-world environments across all robots use one S2E model.** We highly recommend referring to Section A and our demonstration video for more qualitative results and in real environments.

C.3 Ablation on Anchor-based Distribution Matching

We further investigate the influence of the number of anchors used in the S2E model. To systematically study its impact, we conduct an ablation study on the RECON [40] testset by varying the number of anchor points used during both training and inference. All experiments share the same visual encoder, training configuration, and evaluation protocol to ensure fair comparison. Anchor points serve as intermediate spatial targets that guide the policy toward the goal. As shown in Table 7, increasing the number of anchors from 1 to 8 steadily improves performance, reducing minADE and improving mAP. However, adding more anchors beyond this (*e.g.*, 16) does not yield further gains, and even slightly degrades mAP. It suggests that while anchors help structure the navigation plan, an excessive number may introduce redundant intermediate goals, which confuses the policy during inference.

# Anchor	minADE ↓	mAP ↑
1	0.21	0.57
4	0.17	0.58
8	0.13	0.62
16	0.13	0.59

Table 6: Ablation on anchor point number. We vary the number of anchor points used in the S2E model and evaluate on the RECON [40] testset. Increasing the number of anchors improves performance up to a point, with 8 anchors yielding the best results. Adding more anchors beyond this may introduce redundancy or noise, slightly degrading performance.

C.4 Ablation on Visual Encoders

To better understand how the choice of visual encoder influences navigation performance, we conduct an ablation study across several widely used pretrained visual backbones. This ablation is motivated by the observation that, while large-scale vision encoders have demonstrated strong generalization, it remains unclear how well their features can be used to navigation tasks.

Method	minADE ↓	mAP ↑
CLIP [61]	0.13	0.61
DINO-v2 [62]	0.15	0.60
RADIO [63]	0.15	0.58
EfficientNet [64]	0.13	0.62

Table 7: Quantitative results of different visual backbones on the RECON [40] testset. We report minimum Average Displacement Error (minADE) and mean Average Precision (mAP) following standard metrics used in prediction tasks [65]. Surprisingly, the smaller EfficientNet [64] achieves the best performance on both metrics, suggesting that model size and generalization capacity alone do not guarantee better trajectory prediction performance on limited dataset.

As shown in Table 7, we provide evaluation results on RECON [40] testset, using widely used metrics in trajectory prediction tasks [65]. Although models with stronger generalization capabilities based on larger parameters such as RADIO [63] are usually expected to perform better than those smaller ones, our results indicate that their generated trajectories are not always superior. This may

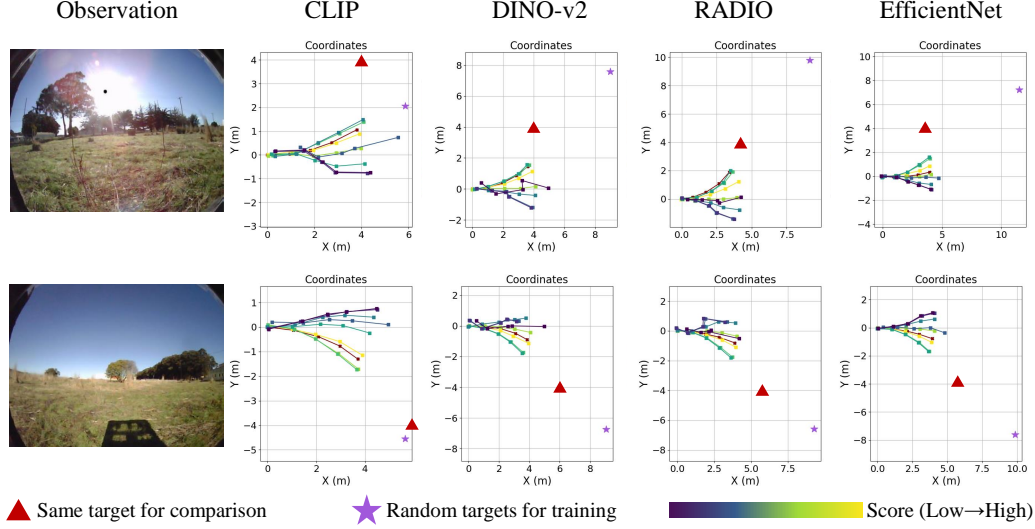


Figure 11: Trajectory visualizations of different visual backbones on the RECON [40] dataset. Each column corresponds to a different visual backbone, and each row shows a different visual observation. The red triangle indicates the same evaluation target across methods, while the purple star denotes random targets used during training. The color gradient along the trajectories indicates the score from low (dark) to high (bright).

be due to several reasons: 1) Larger models are more prone to representation drift when fine-tuned on limited or domain-shifted data pairs; 2) High-capacity models may overfit to semantic context rather than spatial structure; 3) Limited navigation dataset may prevent the policy from effectively leveraging the pretrained features, especially when the visual backbone is not aligned with the task. As shown in Figure 11, the trajectories given by the EfficientNet [64] are much smoother than other backbones. It suggests that a relatively small backbone can support the trajectory prediction reasonably well.

C.5 Qualitative Results on NavBench-GS Benchmark

To enable fair comparison with existing navigation models, we developed the NavBench-GS benchmark, which supports closed-loop evaluation for all navigation policies. Figure 12 presents representative test scenarios from our benchmark. Since these scenes typically lack roadside elements or interactive objects, we construct compositional scenes by adding static obstacles and dynamic pedestrians to increase the complexity and realism of the benchmark scenarios.



Figure 12: Scenes in NavBench-GS Benchmark.

Figure 13 shows comparisons among different variants of S2E in scenes NavBench-GS benchmark. In each scenario, we give the observation and the trajectory of the agent, along with the starting and the goal point. Colored trajectories correspond to different policies—S2E-PPO (red), S2E-BC under

two different control schemes (pink and yellow), and the complete S2E-Full model (cyan). In both scenarios S2E-PPO and S2E-BC either deviate from the intended path or fail to reach the destination, becoming trapped by roadside obstacles or crashing into open space. By contrast, the S2E-Full successfully navigates around obstacles and converges to the goal in all cases, demonstrating its robustness.

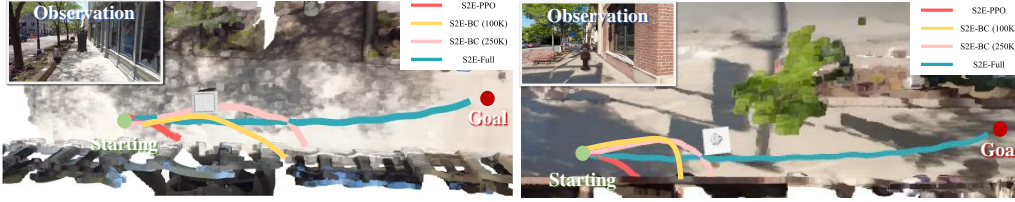


Figure 13: Navigation Trajectories in NavBench-GS Benchmark.

As illustrated in Figure 14, column 1 shows our compositional scenes, where obstacles and pedestrians are overlaid onto base GS environments to simulate complex real-world navigation challenges. Column 2 and 3 demonstrate that NoMaD [11] becomes trapped by roadside obstacles (*e.g.*, traffic lights) or deviates from the intended path, while CityWalker [33] successfully reaches the destination in Scenario 2. Notably, column 4 demonstrates that our method outperforms both approaches, achieving robust navigation in all scenarios containing both static and dynamic obstacles.

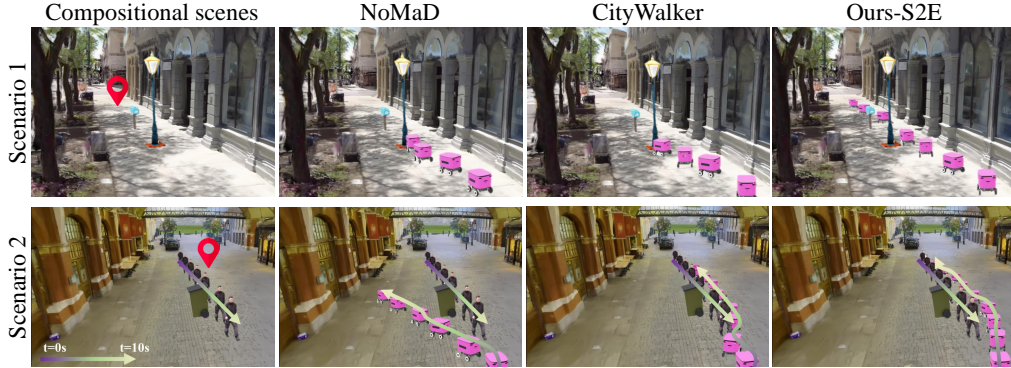


Figure 14: Comparison with SOTAs on NavBench-GS Benchmark.

D Experimental Details

In this section, we provide more details regarding the model architecture, dataset and simulation environments, training strategies, and robots used in our experiments. We begin with a description of the datasets and simulation environments in D.1, followed by the S2E model structure in D.2. D.3 and D.4 describe the pretraining and finetuning strategies, respectively. Finally, Sections D.5 and D.6 introduce the simulated and real-world robotic platforms.

D.1 Details of Dataset and Environments

The S2E training dataset contains over 35 hours of navigation trajectories, sourced entirely from existing real-world records [40, 41] or simulation platforms [43, 44, 59]. The dataset consists of a combination of navigation behaviors collected across 6 distinct robotic platforms, as shown in Table 8 and Figure 15. For real-world datasets, trajectories are labeled using odometry or fused GPS/IMU estimations. In simulation environments, ground-truth poses are directly extracted from the



Figure 15: Examples of dataset for pretraining.



Figure 16: Examples of simulation environments for RL finetuning.

simulator. All data are converted into standardized observation-action pairs by converting applying egocentric transformation.

#	Dataset	Platform	Hrs. Used	Environment
1	RECON [40]	Jackal	25h	off-road
2	SCAND [41]	Spot, Jackal	5h	sidewalks
3	X-Mobility [43, 44]	Nova Carter	2.5h	warehouse
4	URBAN-SIM [59]	COCO, GO2, G1	2.5h	sidewalks

Table 8: Overview of Training Datasets. The table summarizes the robot platforms, environments and useful details covered in each dataset used in S2E pretraining stage.

As shown in Figure 16, we use a diverse set of procedurally generated simulation environments from URBAN-SIM [59] for finetuning. These environments are designed for urban navigation, includ-

ing static obstacles and varying scene layouts. The diversity and randomness in object placement, texture, and lighting encourage robust policy finetuning during reinforcement learning.

D.2 Details of Model Architecture

In this section, we provide details of the model architecture used in S2E, as illustrated in Table 9. We adopt the EfficientNet-B0 convolutional encoder [64], which is pretrained on the ImageNet dataset [66] with a trainable linear layer to tokenize the RGB observations into 768-dimensional embeddings. The goal and anchor vectors are encoded to obtain 768-dimensional embeddings via 2 separate MLPs. To model spatiotemporal relationship, we introduce a Transformer [67]-based architecture consisting of a 4-layer transformer encoder and a 4-layer transformer decoder, each with 8 attention heads and a feedforward dimensionality of 3072 (*i.e.*, 4×768). The encoder processes the sequence of observation tokens with a fixed context size of 5 frames. The decoder takes the combination of observations and goal as keys K and values V while anchor as queries Q to produce action-relevant representations. Finally, the anchor features would be decoded by 3 separate MLPs to obtain normalized trajectories with velocity and score.

Layer	Input [Dimensions]	Output [Dimensions]	Layer Details
1	$\mathbf{o}_{t-k+1:t}$ [5, 3, 320, 640]	$\mathcal{F}_c[:5]$ [5, 768]	Observation token
2	\mathbf{p}_d [1, 2]	$\mathcal{F}_c[5:6]$ [1, 768]	Goal token
3	\mathbf{p}_a [8, 2]	\mathbf{f}_p [8, 768]	Anchor token
4	\mathcal{F}_c [6, 768]	\mathcal{F}'_c [6, 768]	Transformer encoder
5	$K, V = \mathcal{F}'_c$ [6, 768] $Q = \mathbf{f}_p$ [8, 768]	\mathbf{f}'_p [8, 768]	Transformer decoder
6	\mathbf{f}'_p [8, 768]	$[\mu, \sigma]$ [[8, 5, 2], [8, 5, 2]]	Trajectory decoder
7	\mathbf{f}'_p [8, 768]	\mathbf{P} [8, 1]	Score decoder
8	\mathbf{f}'_p [8, 768]	\mathbf{v} [8, 1]	Velocity decoder

Table 9: Architectural Details of the S2E Model. Each row provides the input and output tensor dimensions as well as the specific operation performed at each stage of the model.

D.3 Details of Pretraining

As shown in Table 10, we provide a detailed list of hyperparameter used in pretraining stage of S2E.

S2E Model		S2E Pretraining	
# Parameters	89.4 M	# Epochs n_{ep}	30
RGB Resolution	320×640	Batch Size	64
Encoder	EfficientNet-B0	Learning Rate	2×10^{-4}
Token Dimension	768	Optimizer	AdamW [68, 69]
Attention Hidden Dimension	3072	LR Schedule	Cosine
# Attention Layers n_L	4	Scheduler Period	20
# Attention Heads n_H	8	Compute Resources	$4 \times$ NVIDIA L40S
Temporal Context k	5		
Prediction Horizon T	5		

Table 10: Architectural and Pretraining Hyperparameters for S2E. Left: model architecture. Right: training configuration.

D.4 Details of Finetuning

In this section, we first introduce the finetuning strategy for the GMM-based policy.

First, we observe that the variances of individual actions learned through supervised learning are often excessively small. To address this and encourage exploration during finetuning, we reinitialize the log-standard-deviation (logstd) head to zero.

We use the standard sampling strategy for GMM in RL finetuning. Given the mixture weights $\{q_i\}_{i=1}^M$, means $\{\mu_i\}_{i=1}^M$, and standard deviations $\{\sigma_i\}_{i=1}^M$, an action a is sampled by first selecting a component index $m \sim \text{Categorical}(q)$, then sampling from the corresponding Gaussian:

$$a \sim \mathcal{N}(\mu_m, \sigma_m^2), \quad (6)$$

Since the exact entropy of a GMM does not have a closed-form solution, we use a simplified estimation of its lower bound. First, we approximate it based on the statement of [70, 71]:

$$\mathcal{H}_\pi \approx \sum_{m=1}^M q_m \cdot \left[\frac{1}{2} \log((2\pi e)^2 |\Sigma_m|) \right] - \sum_{m=1}^M q_m \log q_m, \quad (7)$$

$$\Sigma_m = \begin{bmatrix} \sigma_x^{m2} & \rho^m \sigma_x^m \sigma_y^m \\ \rho^m \sigma_x^m \sigma_y^m & \sigma_y^{m2} \end{bmatrix}, \quad (8)$$

we further set $\rho^m = 0$ during finetuning, so we have the estimation:

$$\mathcal{H}_\pi \approx \sum_{m=1}^M q_m \cdot \left[\frac{1}{2} \log((2\pi e)^2 \sigma_x^{m2} \sigma_y^{m2}) \right] - \sum_{m=1}^M q_m \log q_m. \quad (9)$$

We conduct finetuning in URBAN-SIM [59], we train our agent with 256 parallel environments, and the detailed list of hyperparameter used in finetuning stage of S2E is shown in Table 11.

Hyperparameter	Value
# Epochs n_{ep}	300
Minibatch Size	512
Learning Rate	1×10^{-5}
Optimizer	AdamW [68, 69]
LR Schedule	Adaptive
KL Threshold	0.01
Clip Range	0.2
GAE λ	0.95
Discount Factor γ	0.99
Entropy Coefficient	0.001
Rollout Horizon	32
Gradient Clipping	1.5
Value Loss Coefficient	2.0
Compute Resources	1 \times NVIDIA L40S
Finetuning Time	15 hrs

Table 11: S2E PPO Finetuning Hyperparameters. PPO-related training configurations used for finetuning the policy in our experiments.

D.5 Robots in Simulator

All simulated robotic platforms are built upon NVIDIA IsaacSim [72, 73], a high-fidelity and GPU-accelerated simulation environment that supports physics-based interactions and photorealistic rendering. Each robot is modeled using official URDF descriptions and equipped with RGB cameras.

For locomotion, we employ a modular control stack that consists of a low-level joint controller and a high-level policy trained with reinforcement learning. The policy is trained using Proximal Policy Optimization (PPO) on terrain-randomized environments with curriculum learning. The reward function encourages stability, velocity tracking, and energy efficiency, while penalizing collisions and falls. Domain randomization in texture, friction, and mass distribution is applied to improve

sim-to-real transferability. We adopt a shared framework across robot types, enabling scalable embodiment-aware training in simulation.

Wheeled robot. A differential-drive robot, controlled via a kinematic model [74], where linear and angular velocities (v, ω) (calculated from waypoint via a ideal PD controller [11]) are used as control commands. The simulator integrates these commands through rigid-body physics engine, with frictional contacts determining actual wheel-ground interaction.

Unitree-GO2 quadruped robot. A quadruped platform capable of versatile locomotion in complex terrains, the action is a 3-dimensional vector (v_x, v_y, ω) (calculated from waypoint via a ideal PD controller [11]). The locomotion model is a lightweight MLP trained based on the standard training environments provided by IsaacSim [72, 73].

Unitree-G1 humanoid robot. A humanoid agent with articulated head, torso, and leg joints excluding hand actuation, the action is a 3-dimensional vector (v_x, v_y, ω) (calculated from waypoint via a ideal PD controller [11]). The locomotion model is a lightweight MLP trained based on the standard training environments provided by IsaacSim [72, 73].

D.6 Robots in Real World

Wheeled robot. A differential-drive platform equipped with RGB cameras and differential drive odometry, deployed for sidewalk navigation. The robot is controlled via the same kinematic model as in simulation, where linear and angular velocities (v, ω) are computed from waypoints using an ideal PD controller. The odometry is used for real-time position estimation and providing target position during navigation continuously.

Unitree-GO2 quadruped robot. The real-world GO2 robot is equipped with RGB sensors and a low-level locomotion controller provided by Unitree. Instead of executing joint-level commands from a trained policy, we interface with the GO2 through its built-in velocity control API, sending high-level commands (v_x, v_y, ω) to leverage its native gait generation and stability modules. There is a lidar-based odometry used for real-time position estimation and providing target position during navigation continuously.